

Dynamically generated N^* and Λ^* resonances in the hidden charm sector around 4.3 GeV

Jia-Jun Wu^{1,2}, R. Molina^{2,3}, E. Oset^{2,3} and B. S. Zou^{1,3}

¹ Institute of High Energy Physics, CAS, P.O.Box 918(4), Beijing 100049, China

² Departamento de Física Teórica and IFIC, Centro Mixto Universidad de Valencia-CSIC, Institutos de Investigación de Paterna, Aptdo. 22085, 46071 Valencia, Spain

³ Theoretical Physics Center for Science Facilities, CAS, Beijing 100049, China

(Dated: Feb. 2, 2011)

Abstract

The interactions of $\bar{D}\Sigma_c\bar{D}\Lambda_c$, $\bar{D}^*\Sigma_c\bar{D}^*\Lambda_c$, and related strangeness channels, are studied within the framework of the coupled channel unitary approach with the local hidden gauge formalism. A series of meson-baryon dynamically generated relatively narrow N^* and Λ^* resonances are predicted around 4.3 GeV in the hidden charm sector. We make estimates of production cross sections of these predicted resonances in $\bar{p}p$ collisions for PANDA at the forthcoming FAIR facility.

I. INTRODUCTION

The use of chiral Lagrangians in combination with unitary techniques in coupled channels of mesons and baryons has been a very fruitful scheme to study the nature of many hadron resonances. The poles found in the analysis of meson baryon scattering amplitudes are identified with existing baryon resonances. In this way the interaction of the octet of pseudoscalar mesons with the octet of stable baryons has led to $J/P = 1/2^-$ resonances which fit quite well the spectrum of the known low lying resonances with these quantum number [1–5]. The combination of pseudoscalars with the decuplet of baryons has also received attention and also leads to several dynamically generated states [6, 7]. Work substituting pseudoscalar mesons with vector mesons has also been done recently leading to new resonances dynamically generated [8, 9].

One of the interesting findings in the study of the interaction of pseudoscalars with the octet of baryons is the generation of the $N^*(1535)$ resonance which has large couplings to $K\Sigma$ and $K\Lambda$, to the point that the resonance can be approximately considered as a bound state of these meson baryon components [12–14]. Another point of view is that this resonance can be considered as a hidden strangeness state. In fact, phenomenological studies show that, indeed, this seems to be the case [15, 16].

The idea that we want to explore here is to see if one can also generate dynamically baryon states in the hidden charm sector. The interaction of charmed mesons with the octet of stable baryons has been studied in [17, 18] and further refined in [19–21]. Several states with open charm are dynamically generated there, in particular the $\Lambda_c(2593)$.

In the present work we follow the steps of [9, 19] but concentrate in states of hidden charm, for which we study the interaction of an anticharmed meson with a charmed baryon. The underlying theory that we use is an extension to $SU(4)$ of the local hidden gauge Lagrangians [22–25], where $SU(4)$ is broken to account for the different masses of the vector mesons exchanged in the t- and u- channels. The study is done both with pseudoscalar mesons and vector mesons and we obtain three dynamically generated hidden charm baryons generated from the pseudoscalar baryon interaction plus three other states from the interaction of vector mesons with baryons, all of them with masses around 4200-4600 MeV.

We also make estimates of production cross sections with \bar{p} collisions that could be carried out at the future FAIR facility within the PANDA project. We also study how the presence

of these resonances could increase the rate of J/ψ and η_c production around the energies where the resonances can be formed. Part of our results have been briefly reported in [26], here we give a much more complete report of our investigation.

In the next section, we present the formalism and ingredients for the study of the interaction, and give the poles obtained. In the last section, our numerical results are given, followed by a discussion.

II. FORMALISM FOR MESON-BARYON INTERACTION

A. Lagrangian and Feynman diagrams

We consider the $PB \rightarrow PB$ and $VB \rightarrow VB$ interaction by exchanging a vector meson. The corresponding Feynman diagrams are shown in the Fig.1.

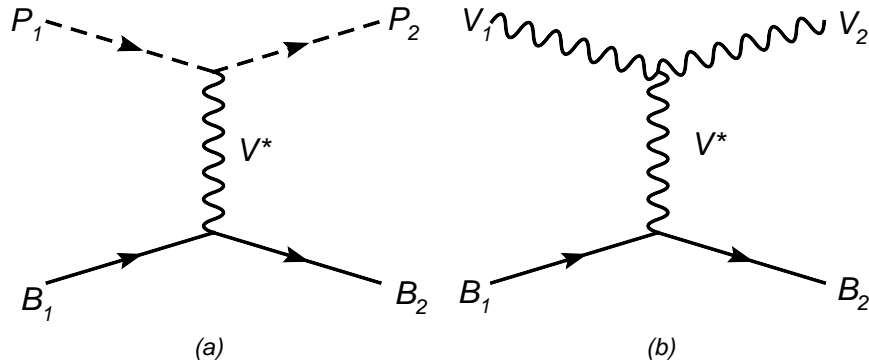


FIG. 1: Feynman diagrams for the pseudoscalar-baryon (a) or vector- baryon (b) interaction via the exchange of a vector meson (P_1, P_2 are D^-, \bar{D}^0 or D_s^-, \bar{D}_s^{*0} , and V_1, V_2 are D^{*-}, \bar{D}^{*0} or D_s^{*-}, \bar{D}_s^{*0} , and B_1, B_2 are $\Sigma_c, \Lambda_c^+, \Xi_c, \Xi'_c$ or Ω_c , and V^* is ρ, K^*, ϕ or ω).

In order to evaluate these Feynman diagrams, we give the three types of vertices for BBV, PPV and VVV interaction from [9]. The Lagrangians for the interaction of vector mesons between themselves (three - vector vertex), pseudoscalar mesons with vectors and baryons with vectors are:

$$\begin{aligned}
 \mathcal{L}_{VVV} &= ig\langle V^\mu[V^\nu, \partial_\mu V_\nu] \rangle \\
 \mathcal{L}_{PPV} &= -ig\langle V^\mu[P, \partial_\mu P] \rangle \\
 \mathcal{L}_{BBV} &= g(\langle \bar{B}\gamma_\mu[V^\mu, B] \rangle + \langle \bar{B}\gamma_\mu B \rangle \langle V^\mu \rangle)
 \end{aligned}
 \tag{1}$$

where B and P are the standard matrices including the pseudoscalar and baryon nonets [27], $g = M_V/2f$ is the coupling used in the hidden gauge with the pion decay constant $f = 93$ MeV and the mass of the light vector meson taken as $M_V = 770$ MeV. The g fulfills the KSFR rule [10] which is tied to vector meson dominance [11]. When we go to SU(4) we can still use the Lagrangian for VPP of Eq. (1) and the V and P matrices extended to SU(4):

$$P = \begin{pmatrix} \frac{\pi^0}{\sqrt{2}} + \frac{\eta_8}{\sqrt{6}} + \frac{\tilde{\eta}_c}{\sqrt{12}} + \frac{\tilde{\eta}'_c}{\sqrt{4}} & \pi^+ & K^+ & \bar{D}^0 \\ \pi^- & -\frac{\pi^0}{\sqrt{2}} + \frac{\eta_8}{\sqrt{6}} + \frac{\tilde{\eta}_c}{\sqrt{12}} + \frac{\tilde{\eta}'_c}{\sqrt{4}} & K^0 & D^- \\ K^- & \bar{K}^0 & \frac{-2\eta_8}{\sqrt{6}} + \frac{\tilde{\eta}_c}{\sqrt{12}} + \frac{\tilde{\eta}'_c}{\sqrt{4}} & D_s^- \\ D^0 & D^+ & D_s^+ & -\frac{3\tilde{\eta}_c}{\sqrt{12}} + \frac{\tilde{\eta}'_c}{\sqrt{4}} \end{pmatrix}, \quad (2)$$

and

$$V_\mu = \begin{pmatrix} \frac{\rho^0}{\sqrt{2}} + \frac{\omega_8}{\sqrt{6}} + \frac{\tilde{\omega}_c}{\sqrt{12}} + \frac{\tilde{\omega}'_c}{\sqrt{4}} & \rho^+ & K^{*+} & \bar{D}^{*0} \\ \rho^- & -\frac{\rho^0}{\sqrt{2}} + \frac{\omega_8}{\sqrt{6}} + \frac{\tilde{\omega}_c}{\sqrt{12}} + \frac{\tilde{\omega}'_c}{\sqrt{4}} & K^{*0} & D^{*-} \\ K^{*-} & \bar{K}^{*0} & \frac{-2\omega_8}{\sqrt{6}} + \frac{\tilde{\omega}_c}{\sqrt{12}} + \frac{\tilde{\omega}'_c}{\sqrt{4}} & D_s^{*-} \\ D^{*0} & D^{*+} & D_s^{*+} & -\frac{3\tilde{\omega}_c}{\sqrt{12}} + \frac{\tilde{\omega}'_c}{\sqrt{4}} \end{pmatrix}_\mu. \quad (3)$$

Let us recall that here $\tilde{\eta}_c$ stands for the SU(3) singlet of the 15th SU(4) representation and we denote $\tilde{\eta}'_c$ for the singlet of SU(4). On the other hand, ω_8 plays the role of the η_8 for the vectors, while $\tilde{\omega}_c$ the role of $\tilde{\eta}_c$, and we denote by $\tilde{\omega}'_c$ the SU(4) singlet. We take π^0 , η , η' , η_c as a basis for the neutral pseudoscalar mesons, where η' is the singlet in SU(3), $(u\bar{u} + d\bar{d} + s\bar{s})/\sqrt{3}$, and η_c stand for $c\bar{c}$. Recalling the standard quark composition of the

SU(4) mesons

$$\begin{aligned}
\pi^0 &= \frac{1}{\sqrt{2}}(u\bar{u} - d\bar{d}) \\
\eta_8 &= \frac{1}{\sqrt{6}}(u\bar{u} + d\bar{d} - 2s\bar{s}) \\
\tilde{\eta}_c &= \frac{1}{\sqrt{12}}(u\bar{u} + d\bar{d} + s\bar{s} - 3c\bar{c}) \\
\tilde{\eta}'_c &= \frac{1}{\sqrt{4}}(u\bar{u} + d\bar{d} + s\bar{s} + c\bar{c}) ,
\end{aligned} \tag{4}$$

we find

$$\begin{aligned}
\eta_8 &= \eta \\
\eta' &= \frac{1}{2}\tilde{\eta}_c + \frac{\sqrt{3}}{2}\tilde{\eta}'_c \\
\eta_c &= \frac{1}{2}(-\sqrt{3}\tilde{\eta}_c + \tilde{\eta}'_c) ,
\end{aligned} \tag{5}$$

in the physical basis. On the other hand, for vectors we use the physical basis ρ^0 , ω , ϕ and J/ψ , where

$$\begin{aligned}
\rho^0 &= \frac{1}{\sqrt{2}}(u\bar{u} - d\bar{d}) \\
\omega &= \frac{1}{\sqrt{2}}(u\bar{u} + d\bar{d}) \\
\phi &= s\bar{s} \\
J/\psi &= c\bar{c} ,
\end{aligned} \tag{6}$$

which can be written in terms of ω_8 , $\tilde{\omega}_c$ and $\tilde{\omega}'_c$ as¹

$$\begin{aligned}
\omega &= \frac{1}{6}(\sqrt{6}\tilde{\omega}_c + 2\sqrt{3}\omega_8 + 3\sqrt{2}\tilde{\omega}'_c) \\
\phi &= \frac{1}{6}(\sqrt{3}\tilde{\omega}_c - 2\sqrt{6}\omega_8 + 3\tilde{\omega}'_c) \\
J/\psi &= \frac{1}{2}(-\sqrt{3}\tilde{\omega}_c + \tilde{\omega}'_c) .
\end{aligned} \tag{7}$$

The use of Lagrangians to give the BBV vertex in SU(4) is more cumbersome than in SU(3) and thus it is simpler to use SU(4) Clebsch Gordan coefficients. Yet, this requires a certain phase convention for the physical states with respect to the isospin states implicit in the

[1] Latter on, in order to use the SU(4) Clebsch Gordan coefficients we shall change a phase to the $\tilde{\eta}_c$ and $\tilde{\omega}_c$.

SU(4) tables, which makes convenient to use the same procedure to evaluate the PPV vertex.

In the PPV vertex we go from the $15 \otimes 15$ representation of pseudoscalars to the 15 representation of vectors. Yet, the nature of the couplings (with the explicit commutator) has as a consequence that only the 15_F (antisymmetric) representation for the vectors is needed (one can alternatively use explicitly the 15_F and the 15_D representations and the 15_D contribution vanishes at the end²). The resulting t amplitude for $P_1 P_2 \rightarrow V$ is given by

$$t_{P_1 P_2 V} = g_{15_F} C_{15_F}(15 \otimes 15) (q_1 + q_2) \cdot \epsilon , \quad (8)$$

where q_1 and q_2 are the four-momentum of the initial and final pseudoscalar mesons respectively, and $C_{15_F}(15 \otimes 15)$ is the SU(4) Clebsch Gordan Coefficient that we take from [28] and g_{15_F} is the reduced matrix element that by comparison with the result of the Lagrangian is given by

$$g_{15_F} = -2\sqrt{2}g . \quad (9)$$

However, the use of the SU(4) tables requires a phase convention. We find a compatible and convenient phase convention of the isospin states implicit in the SU(4) tables and those used by us in Eqs. (8) and (9) by means of:

$$|K^0\rangle = -|1/2, -1/2\rangle ; \quad |\pi^+\rangle = -|1, 1\rangle ; \quad |\pi^0\rangle = -|1, 0\rangle ;$$

$$|D_s^+\rangle = -|0, 0\rangle ; \quad |\bar{D}^0\rangle = -|1/2, 1/2\rangle ; \quad |\tilde{\eta}_c\rangle = -|0, 0\rangle ;$$

and equivalent phases for the corresponding vectors, K^{*0} , ρ^+ , ρ^0 , D_s^{*+} , \bar{D}^{*0} and $\tilde{\omega}_c$. The necessity for the change in phases stems from demanding that the $15 \otimes 15 \rightarrow 1$ combination of SU(4) isospin states is a symmetrical expression in the physical states [29]. The use of this convention (and also the convention for baryons that we give later) leads to the same amplitudes in charge basis given by the Lagrangians of Eq. (1) with the P and B matrices written in the SU(3) basis.

When we go to the BBV vertex (we look for $B\bar{B} \rightarrow V$), we need now the three representations, 15_1 , 15_2 and 1, and we must note that when the 8 representation of SU(3) is involved, only the F coefficients are needed. In this case we have $20' \otimes \bar{20}' \rightarrow 15_1, 15_2, 1$, and

[2] We thank J. Nieves for pointing this to us.

the t amplitude for the BBV vertex is given by

$$t_{B_1 \bar{B}_2 V} = \{g_{15_1} C_{15_1}(20' \otimes \bar{20}') + g_{15_2} C_{15_2}(20' \otimes \bar{20}') + g_1 C_1(20' \otimes \bar{20}')\} \bar{u}_{r'}(p_2) \gamma \cdot \epsilon u_r(p_1) . \quad (10)$$

Once again by writing the expression for $20' \otimes \bar{20}' \rightarrow 1$ in terms of the SU(4) isospin states, and demanding that the expression is symmetrical in the physical baryons, we obtain a convention of phases. The one we have chosen, partly motivated to agree formally with earlier SU(3) results, is given by changing the phases of the states

$$\begin{aligned} |\bar{\Xi}_{cc}^{--}\rangle &= -|1/2, -1/2\rangle , & |\Omega_{cc}^+\rangle &= -|0, 0\rangle , & |\Xi_c^0\rangle &= -|1/2, -1/2\rangle , & |\bar{\Xi}_c^0\rangle &= -|1/2, -1/2\rangle , \\ |\bar{\Lambda}_c^-\rangle &= -|0, 0\rangle , & |\Sigma_c^+\rangle &= -|1, 0\rangle , & |\Sigma_c^{++}\rangle &= -|1, 1\rangle , & |\bar{\Sigma}_c^{--}\rangle &= -|1, -1\rangle , \\ |n\rangle &= -|1/2, -1/2\rangle , & |\bar{\Xi}^0\rangle &= -|1/2, -1/2\rangle , & |\bar{\Sigma}^+\rangle &= -|1, 1\rangle , & |\Sigma^+\rangle &= -|1, 1\rangle , \\ |\Sigma^0\rangle &= -|1, 0\rangle , & |\bar{\Sigma}^0\rangle &= -|1, 0\rangle . \end{aligned}$$

The reduced matrix elements of Eq. (10), g_{15_1} , g_{15_2} and g_1 are evaluated demanding:

- 1) The coupling $p\bar{p} \rightarrow J/\psi$ should be zero by OZI rules,
- 2) The coupling $p\bar{p} \rightarrow \phi$ should be zero by OZI rules,
- 3) The coupling $p\bar{p} \rightarrow \rho^0$ should be the one obtained in SU(3).

We finally obtain

$$g_{15_1} = -g; \quad g_{15_2} = 2\sqrt{3}g; \quad g_1 = 3\sqrt{5}g . \quad (11)$$

with $g = M_V/2f$ and $f = 93MeV$ the pion decay constant.

The diagram of Fig. 1 (a) requires the exchange of the vector meson with the two vertices given by Eqs. (8) and (10). In the sum of polarizations in the vector meson exchanged,

$$\sum_{\lambda} \epsilon_{\mu} \epsilon_{\nu} = -g_{\mu\nu} + \frac{q_{\mu} q_{\nu}}{M_V^2} . \quad (12)$$

We can keep just the $\mu = \nu = 0$ component since we assume that the three momenta of the particles are small compared to their masses. Similarly, the q^2/M_V^2 term in the vector meson

propagator is neglected (further on, when we consider the transitions from heavy mesons to light ones, we perform the exact calculation). The transition potential corresponding to the diagrams of Fig. 1 are given by

$$V_{ab(P_1 B_1 \rightarrow P_2 B_2)} = \frac{C_{ab}}{4f^2}(q_1^0 + q_2^0), \quad (13)$$

$$V_{ab(V_1 B_1 \rightarrow V_2 B_2)} = \frac{C_{ab}}{4f^2}(q_1^0 + q_2^0)\vec{\epsilon}_1 \cdot \vec{\epsilon}_2. \quad (14)$$

Where the indices a, b stand for different groups of $P_1(V_1)B_1$ and $P_2(V_2)B_2$, respectively. The q_1^0, q_2^0 are the energies of the initial, final meson. We list the value of the C_{ab} coefficients for different states of isospin, I, and strangeness, S in the Appendix. Here we study six different cases with $(I, S) = (3/2, 0), (1/2, 0), (1/2, -2), (1, -1), (0, -1), (0, -3)$.

B. The G function and the unitary T amplitudes

The G function is a loop function of a meson (P) and a baryon(B) which we calculate in dimensional regularization by means of the formula

$$\begin{aligned} G_{(P,B)} &= i2M_B \int \frac{d^4q}{(2\pi)^4} \frac{1}{(P-q)^2 - M_B^2 + i\epsilon} \frac{1}{q^2 - M_P^2 + i\epsilon}, \quad (15) \\ &= \frac{2M_B}{16\pi^2} \left\{ a_\mu + \ln \frac{M_B^2}{\mu^2} + \frac{M_P^2 - M_B^2 + s}{2s} \ln \frac{M_P^2}{M_B^2} \right. \\ &\quad + \frac{\bar{q}}{\sqrt{s}} [\ln(s - (M_B^2 - M_P^2) + 2\bar{q}\sqrt{s}) + \ln(s + (M_B^2 - M_P^2) + 2\bar{q}\sqrt{s}) \\ &\quad \left. - \ln(-s - (M_B^2 - M_P^2) + 2\bar{q}\sqrt{s}) - \ln(-s + (M_B^2 - M_P^2) + 2\bar{q}\sqrt{s})] \right\}, \quad (16) \end{aligned}$$

where

$$s = P^2, \quad (17)$$

$$\bar{q} = \frac{\sqrt{(s - (M_B + M_P)^2)(s - (M_B - M_P)^2)}}{2\sqrt{s}} \quad \text{with } \text{Im}(q) > 0. \quad (18)$$

In Eq. (16), q is the four-momentum of the meson, and P is the total four-momentum of the meson and the baryon. The μ is a regularization scale, which we put 1000 MeV, and a_μ is of the order of -2 , which is the natural value of the subtraction constant [3]. When we look for poles in the second Riemann sheet, we must change q by $-q$ when \sqrt{s} is above the threshold in Eq. (16) [30]. See further comments regarding the subtraction constant in Subsection D.

Here we also regularize the G loop function in a different way by putting a cutoff in the three-momentum. The formula is:

$$\begin{aligned} G_{(P,B)} &= i2M_B \int \frac{d^4q}{(2\pi)^4} \frac{1}{(P-q)^2 - M_B^2 + i\epsilon} \frac{1}{q^2 - M_P^2 + i\epsilon} \\ &= \int_0^\Lambda \frac{q^2 dq}{4\pi^2} \frac{2M_B(\omega_P + \omega_B)}{\omega_P \omega_B ((P^0)^2 - (\omega_P + \omega_B)^2 + i\epsilon)}, \end{aligned} \quad (19)$$

where

$$\begin{aligned} \omega_P &= \sqrt{\vec{q}^2 + M_P^2}, \\ \omega_B &= \sqrt{\vec{p}^2 + M_B^2}, \end{aligned} \quad (20)$$

and Λ is the cutoff parameter in the three-momentum of the function loop.

For these two types of G function, the free parameters are a_μ in Eq. (16) and Λ in Eq. (19). When we choose a_μ or Λ , the shapes of these two functions are almost the same close to threshold and they take the same value at threshold.

Then we can get the unitary T amplitudes by solving the coupled channels Bethe-Salpeter equation in the on shell factorization approach of [3, 31, 32]

$$T = [1 - VG]^{-1}V. \quad (21)$$

When we look for poles in the complex plane of \sqrt{s} , poles in the T matrix that appear in the first Riemann sheet below threshold are considered as bound states whereas those located in the second Riemann sheet and above the threshold of some channel are identified as resonances.

C. The coupling constant and the width of the poles

From the T matrix we can find the pole positions z_R . In this work, we find all of these poles in the real axes below threshold, in a few words, they are bound states. In view of that, for these cases the coupling constants are obtained from the amplitudes in the real axis. These amplitudes behave close to the pole as:

$$T_{ab} = \frac{g_a g_b}{\sqrt{s} - z_R}. \quad (22)$$

We can get the coupling constant as:

$$g_a^2 = \lim_{\sqrt{s} \rightarrow z_R} (T_{aa} \times (\sqrt{s} - z_R)). \quad (23)$$

This expression allows us to determine the value of g_a , except by a global phase. Then, the other couplings are derived from

$$g_b = \lim_{\sqrt{s} \rightarrow z_R} \left(\frac{g_a T_{ab}}{T_{aa}} \right). \quad (24)$$

As all the states that we find have zero width, we should take into account some decay mechanisms. Thus, we consider the decay of the states to light meson - light baryon by means of box diagrams as it was done in [33, 34]. The Feynman diagrams for these decays are shown in Fig. 2. We assume that P_3 , V_3 and B_3 are on-shell and neglect the three-momentum of the initial and final particles. Then, using Eq. (1), the transition potential of these diagrams can be written as:

$$\begin{aligned} V_{acb(P_1 B_1 \rightarrow P_3 B_3 \rightarrow P_2 B_2)} &= \frac{C_{ac} C_{cb} M_{V^*}^4}{16 f^4} \times G_{(P_3, B_3)} \times \frac{(\sqrt{s} + M_{B_3})^2 - M_{P_3}^2}{4 \sqrt{s} M_{B_3}} \\ &\times \frac{-2E_{P_1} + (M_{B_3} - M_{B_1})(M_{P_1}^2 + M_{V_1^*}^2 - M_{P_3}^2)/M_{V_1^*}^2}{M_{P_1}^2 + M_{P_3}^2 - 2E_{P_3} E_{P_1} - M_{V_1^*}^2} \\ &\times \frac{-2E_{P_2} + (M_{B_3} - M_{B_2})(M_{P_2}^2 + M_{V_2^*}^2 - M_{P_3}^2)/M_{V_2^*}^2}{M_{P_2}^2 + M_{P_3}^2 - 2E_{P_3} E_{P_2} - M_{V_2^*}^2}, \quad (25) \end{aligned}$$

and the same for vectors (see Fig. 2. (b)) changing E_{P_1} , E_{P_2} , E_{P_3} by E_{V_1} , E_{V_2} , E_{V_3} and M_{P_1} , M_{P_2} , M_{P_3} by M_{V_1} , M_{V_2} , M_{V_3} , respectively. Here c stands for a different group of $P_3(V_3)B_3$. Then, the kernel V in the Bethe Salpeter equation, Eq. (21), becomes now:

$$V_{ab(P_1 B_1 \rightarrow P_2 B_2)} = \frac{C_{ab}}{4 f^2} (E_{P_1} + E_{P_2}) + \sum_c V_{acb}, \quad (26)$$

and similarly for the VB system. In Eq. (25) we have factorized the two $P_1 B_1 \rightarrow P_3 B_3$ and $P_3 B_3 \rightarrow P_2 B_2$ transition amplitudes outside the loop integral by taking their values when the system $P_3 B_3$ is set on-shell. This is a good approximation, exact for the imaginary part of the diagram, which is our main concern, since we are interested in the contribution of these diagrams to the width of the resonances. The loop integral only affects then the P_3 , B_3 propagators leading to the same G function defined in Eq. (16). Since the on-shell mass of the intermediate states is far away from the energies investigated, $\text{Re}G(P_3, B_3)$ is small and we have checked that it is sufficiently smaller than the tree level contribution from the diagrams of Fig. (1), such that it can be ignored. For example, $V_{(\bar{D}\Sigma_c \rightarrow \pi N \rightarrow \bar{D}\Sigma_c)} = (0.38 + 2.9i) \text{ GeV}^{-1}$ at the N^* pole position with $\sqrt{s} = 4.265 \text{ GeV}$.

Further on, we will include the $\eta_c N$, $\eta_c \Lambda$ channels for $PB \rightarrow PB$, and $J/\psi N$, $J/\psi \Lambda$ for $VB \rightarrow VB$ in the calculation.

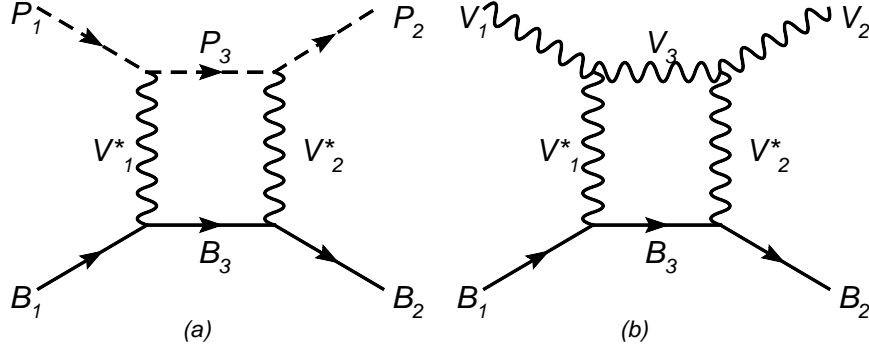


FIG. 2: The Feynman diagrams of pseudoscalar-baryon (a) or vector-baryon (b) interaction via a box diagram. $P_1, P_2, V_1, V_2, B_1, B_2$ are the same particles than in Fig. 1. P_3, V_3 and B_3 are light particles belonging to the SU(3) octet of pseudoscalar mesons, vector mesons and stable baryons, respectively, and V_1^*, V_2^* are D^* or D_s^* .

D. Discussion about the use of the SU(4) flavor symmetric Lagrangian

Once the formalism has been exposed we would like to make some comments to justify the approach. While the hidden local gauge approach is well settled with SU(3) flavor, its extension to SU(4) is not quite justified. The local hidden gauge theory in QCD is based on spontaneous symmetry breaking of chiral symmetry, which is not expected to hold in the charmed sector, and even if this were the case, the breaking pattern would be masked by the large charm mass. In view of this, the approach followed requires some justification. The first thing we must bare in mind is that the large mass of the charmed quark is to be blamed for the lack of symmetry. Hence, if hadron dynamics still has some traces of SU(4) symmetry it should be in particular vertices or amplitudes not tied to the quark mass. In this respect it is interesting to mention that SU(4) symmetry works fairly well for the vertices $VP\gamma$ (or equivalently the VVP) involved in the radiative decay of vector mesons with charm to a pseudoscalar and a photon [35]. The agreement is as good as in SU(3). Given the analogies between the VVP and VVV vertices provided by heavy quark symmetry, it is fair to think that using SU(4) symmetry to evaluate the VVV and VPP vertices would be a fair starting point. Similarly we could also assume the same symmetry to hold in the VBB vertices.

One should also note that in the case of meson meson interaction the present approach provides the same results, up to a mass term of no practical consequences, as the heavy quark

formalism used in [36–38] for the case of interaction of light mesons with heavy meson. From the perspective of our approach, we could rephrase it by stating that these two approaches provide the same VVV (or VPP) vertices with two heavy vectors and a light one. For the evaluation of the width in the present approach one is using these vertices, with the only difference with respect to [36–38] that one of the heavy vectors is exchanged in the t -channel in our approach, while the two heavy vectors (or pseudoscalars) were external particles in [36–38]. Only vertices involving three heavy vectors (D^*D^*J/ψ) would require the extra help of SU(4) symmetry. Thus, most of the information used is supported by phenomenology and other approaches.

Furthermore, we should bare in mind that the largest fraction of the results that we obtain, concerning couplings to different channels, is based on SU(3), since we can relate these channels through SU(3). Then, implementing SU(4) symmetry as we do, automatically accomplishes this. Only when we give a jump to another charm sector the SU(4) symmetry would play a role and there we would invoke the arguments used above to support it. Certainly, when these vertices are used in Feynmann diagrams and the masses of the exchanged vectors are very different, the approximate SU(4) symmetry that we had in the vertices will be badly broken in the amplitudes. This happens also in SU(3): The vertices are manifestly SU(3) invariant, but when SU(3) is broken in the amplitudes because of the different masses of the particles belonging to the same multiplet (for instance in the unitarization procedure), the underlying SU(3) symmetry is broken and two octets that were degenerate in the exact SU(3) limit give rise to two different states in the strangeness $S = -1$ sector: one of the two $\Lambda(1405)$ states and the $\Lambda(1670)$.

Yet, one should be ready to accept larger uncertainties than in SU(3) and allow some fitting freedom in the approach. This can be done by means of the subtraction constants of the G function, that effectively tune the strength of the potentials that one is using in the approach. This also means that the natural values of these constants should only be used as indicative and then a real fit to the data should be done, which cannot be done in the present case since we have no experimental data. However, one can rely on previous work along these lines in which several groups have done this work and provide the new scale of the subtraction constants to be used in the charm sector. In this sense, the works of [19, 39–42], choosing these parameters to reproduce properties of known resonances like the $D_{s0}^0(2317)$, the X(3872), the $D_2^*(2460)$ and $D^*(2640)$, and $\Lambda_c(2593)$, have given us the

scale for these subtractions constants that we use here.

III. RESULT AND DISCUSSION

A. The pole positions and coupling constants

Here we show the results for the different sectors. By using the two G functions of Eqs. (16) and (19), the poles appear in both cases below threshold in the first Riemann sheet and therefore they are bound states. We show the pole positions for different values of $\alpha(\Lambda)$ in Tables I and II.

We take a range of values of α , or accordingly the cut off, in line with values used in [19, 39–41] and we find six poles in our calculation. The uncertainties in the pole positions in the case of the first and third poles for both PB and VB systems, are of the order of 100 MeV, which are typical in any hadron model. These two poles are rather stable. However, for the second state, the uncertainties are much larger and the pole position is very unstable.

For the discussions that follow we choose an intermediate value of α , which we take $\alpha = -2.3$, to study the nature of these poles in detail. In Tables III and IV, the values of the coupling constants are listed by using Eqs. (23) and (24). From Table III, we see that both the $N^*(4269)$ and the $\Lambda^*(4403)$ depend on one channel, $\bar{D}\Sigma_c$ and $\bar{D}\Xi'_c$, respectively. These two states are both stable as we can see in Table I. In contrast, the $\Lambda^*(4213)$ depend on two channels, $\bar{D}_s\Lambda_c^+$ and $\bar{D}\Xi_c$. The mass of this state changes appreciably by using different values of the free parameters (α or Λ).

B. The decay widths of these states to light meson - light baryon channels

These states decay to two different types of channels, one is the light meson - light baryon channel, while the other is the $c\bar{c}$ meson - baryon channel. For the VB states, there is another possibility to decay into PB channels, for instance, $\bar{D}^*B \rightarrow \bar{D}B$. The analogous decay channels in the $VV \rightarrow VV$ hidden charm sector driven by pseudoscalar exchange were studied in [43] and found to be extremely small because of the small phase space available. Analogously, the terms involving a vector exchange contains an anomalous VVP vertex and were also found very small in [33]. Hence, we do not consider them here. In this subsection

(I, S)	$\alpha = -2.2(\Lambda = 0.7 \text{ GeV})$	$\alpha = -2.3(\Lambda = 0.8 \text{ GeV})$	$\alpha = -2.4(\Lambda = 0.9 \text{ GeV})$
	z_R	z_R	z_R
(1/2, 0)	4291(4273)	4269(4236)	4240(4187)
(0, -1)	4247(4120)	4213(4023)	4170(3903)
	4422(4394)	4403(4357)	4376(4308)

TABLE I: Pole position from $PB \rightarrow PB$ using the two different G functions of Eqs. (16) and (19). The units are in MeV.

(I, S)	$\alpha = -2.2(\Lambda = 0.7 \text{ GeV})$	$\alpha = -2.3(\Lambda = 0.8 \text{ GeV})$	$\alpha = -2.4(\Lambda = 0.9 \text{ GeV})$
	z_R	z_R	z_R
(1/2, 0)	4438(4410)	4418(4372)	4391(4320)
(0, -1)	4399(4256)	4370(4155)	4330(4030)
	4568(4532)	4550(4493)	4526(4441)

TABLE II: Pole position from $VB \rightarrow VB$ using the two different G functions of Eqs. (16) and (19). The units are in MeV.

we only consider the decay of these states to the light meson - light baryon channel as depicted in the Feynman diagrams of Fig. 2. These diagrams provide a negligible real part compared to the tree level potentials. The imaginary part gives rise to a width of the states. Hence, we only consider the effect of this box diagram on the states found before.

In Figs. 3 and 4, we show the results of $|T_{ii}|^2$ as a function of \sqrt{s} for the different channels, and we list their decay widths to the different channels for all the sectors in Tables V and VI. From these pictures and tables, we find that the six states are all above 4200 MeV. However, their widths are quite small. In principle, one might think that the width of these massive objects should be large because there are many channels open and there is much phase space for decay. However, it is difficult for the $c\bar{c}$ components to decay to the $u\bar{u}$, $d\bar{d}$ and $s\bar{s}$ ones, something that within our model is tied to the necessity of the exchange of a heavy - vector meson. Note that the pole positions are obtained without including the box diagrams by extrapolating to the complex plane. The inclusion of the box diagram renders

(I, S)	z_R (MeV)	g_a		
(1/2, 0)		$\bar{D}\Sigma_c$	$\bar{D}\Lambda_c^+$	
	4269	2.85	0	
(0, -1)		$\bar{D}_s\Lambda_c^+$	$\bar{D}\Xi_c$	$\bar{D}\Xi'_c$
	4213	1.37	3.25	0
	4403	0	0	2.64

TABLE III: Pole positions, z_R and coupling constants, g_a , for the states from $PB \rightarrow PB$.

(I, S)	z_R (MeV)	g_a		
(1/2, 0)		$\bar{D}^*\Sigma_c$	$\bar{D}^*\Lambda_c^+$	
	4418	2.75	0	
(0, -1)		$\bar{D}_s^*\Lambda_c^+$	$\bar{D}^*\Xi_c$	$\bar{D}^*\Xi'_c$
	4370	1.23	3.14	0
	4550	0	0	2.53

TABLE IV: Pole position and coupling constants for the bound states from $VB \rightarrow VB$.

this extrapolation more difficult, and thus we obtain the width of the states by plotting $|T|^2$ versus the energy with T obtained in the real axis including the box diagrams. The individual partial decay widths are obtained including one by one the different box diagrams.

C. Decay width to $c\bar{c}$ meson - light baryon channels

In this subsection we discuss the decay width of these states to $c\bar{c}$ meson and light - baryon channels. The three states from the VB system decay to $J/\psi N$. The decay of these VB states to $\eta_c N$ is also possible by means of a BBP vertex (exchange of a pseudoscalar meson) but as we will see in the Subsection IV. B this vertex is very small. We could also have this decay exchanging a vector meson instead of a pseudoscalar one, but then the amplitude would contain an anomalous VVP vertex, which is also very small [33]. Similarly, the decay width of the PB states to the VB channels must be very small because of the same reasons. We will consider their decay to $J/\psi N$ in Section IV. B and we anticipate that this decay

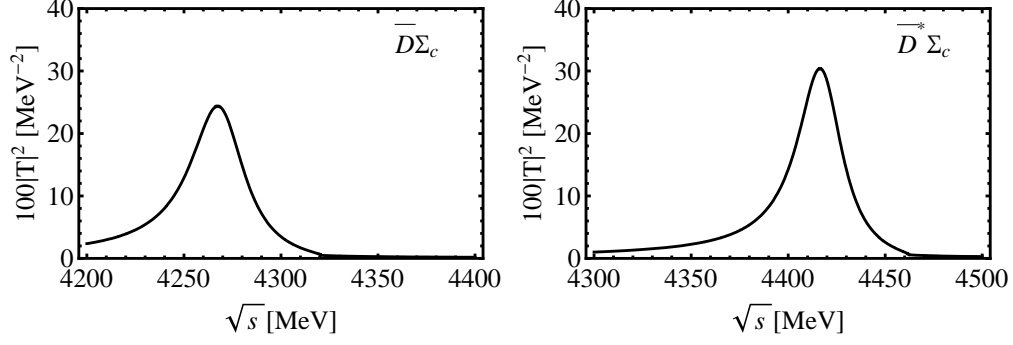


FIG. 3: $|T_{ii}|^2$ for the different channels in the $(I = 1/2, S = 0)$ sector including the box diagrams.

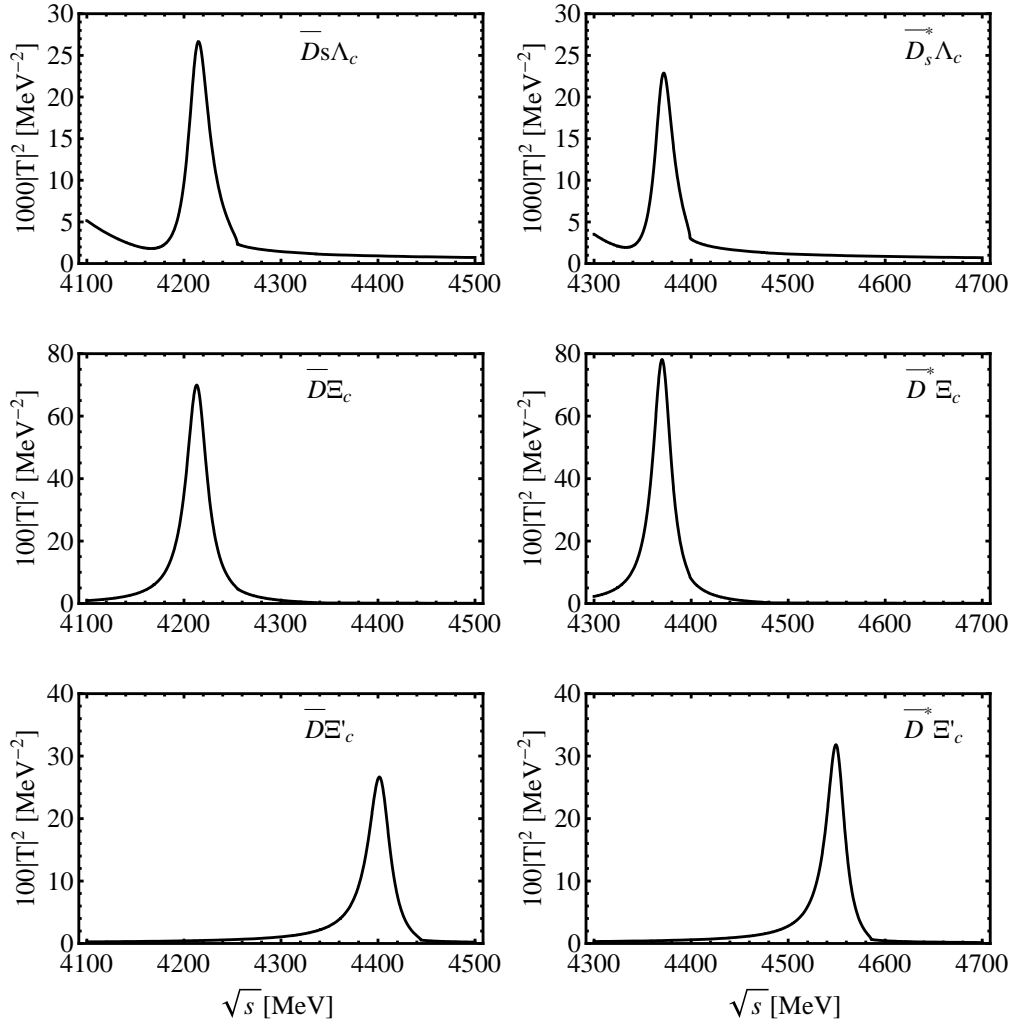


FIG. 4: $|T_{ii}|^2$ for the different channels in the $(I = 0, S = -1)$ sector including the box diagrams.

(I, S)	z_R	Real axis		Γ_i				
		M	Γ					
$(1/2, 0)$				πN	ηN	$\eta' N$	$K\Sigma$	
	4269	4267	34.3	3.8	8.1	3.9	17.0	
$(0, -1)$				$\bar{K}N$	$\pi\Sigma$	$\eta\Lambda$	$\eta'\Lambda$	$K\Xi$
	4213	4213	26.4	15.8	2.9	3.2	1.7	2.4
	4403	4402	28.2	0	10.6	7.1	3.3	5.8

TABLE V: Pole position (z_R), mass (M), total width (Γ), and the decay width for each particular light meson - light baryon channel (Γ_i) for the states from $PB \rightarrow PB$. The units are in MeV.

(I, S)	z_R	Real axis		Γ_i				
		M	Γ					
$(1/2, 0)$				ρN	ωN	$K^*\Sigma$		
	4418	4416	28.4	3.2	10.4	13.7		
$(0, -1)$				\bar{K}^*N	$\rho\Sigma$	$\omega\Lambda$	$\phi\Lambda$	$K^*\Xi$
	4370	4371	23.3	13.9	3.1	0.3	4.0	1.8
	4550	4549	23.7	0	8.8	9.1	0	5.0

TABLE VI: Pole position (z_R), mass (M), total width (Γ), and the decay width for each particular light meson - light baryon channel (Γ_i) for the states from $PB \rightarrow PB$. The units are in MeV.

width is very small. For these reasons, we only consider the $J/\psi N$, $J/\psi\Lambda$ channels for the VB states, and $\eta_c N$, $\eta_c\Lambda$ channels in the case of states from the PB system. Thus, these new channels are added to the previous calculation in the Subsections III. A and B.

The pole positions of these states only change a bit compared to those given in the Subsection III. A, since the potentials from these channels are much smaller. Nevertheless, these channels provide some extra width because, in spite of the smaller phase space for the decay, the three momentum transfer in the propagator of the $D^*(D_s^*)$ exchange is much smaller than in the case of transition to light meson - light baryon channels. The transition

potential becomes:

$$V_{ab(PB \rightarrow \eta_c B)} = -\frac{C_{ab} g^2}{p_{D^*}^2 - M_{D^*}^2} (E_P + E_{\eta_c}) , \quad (27)$$

where

$$p_{D^*}^2 = M_{\eta_c}^2 + M_P^2 - 2E_{\eta_c} E_P , \quad (28)$$

and similarly for the VB system but changing p_{D^*} , M_{D^*} , E_P and E_{η_c} by p_D , M_D , E_V and $E_{J/\psi}$ respectively. Here we also neglect the three-momentum of the final and initial particles because we consider energies close to the threshold. We list the results in Tables VII, VIII, IX and X. We observe that the coupling constants change a bit, but what is more relevant is that these new channels give an extra contribution to the width, smaller, but of the same order as the one obtained previously. The relatively large decay width to the $\eta_c N$ channel is a good feature with respect to the possible observation of these resonances since there will be less background in $\eta_c N$ than in πN , ηN , $K\Sigma$, the observation of the resonance in the $\eta_c N$ channel could be favoured.

In Tables VII and VIII, the pole positions are obtained without the box diagrams, but including the $\eta_c N$, $\eta_c \Lambda$ channels. Now the pole positions becomes complex because the new channels are open. We can see that the partial decay width into these channels is approximately twice the imaginary part of the pole position. The total widths are again obtained by looking at the width of $|T|^2$ in the real axis when the box diagrams are included. We would like to mention that in the approach of [18], which has been corrected in [19, 20], some hidden charm states are also found, bound by about 1000 MeV. It is not easy to understand such a large binding on physical grounds, which is not supported in any case by the strength of the potentials.

IV. PRODUCTION CROSS SECTION IN $\bar{p}p$ COLLISIONS

A. Estimate of the $\bar{p}p \rightarrow N_{c\bar{c}}^{*+}(4265)\bar{p}$ cross section

We shall estimate the production cross section of these resonances at FAIR. With a \bar{p} beam of 15 GeV/c one has $\sqrt{s} = 5470$ MeV, which allows one to observe resonances in $\bar{p}X$ production up to a mass $M_X \simeq 4538$ MeV. We shall make some rough estimate of the cross section for the $\bar{p}p \rightarrow \bar{p}N_{c\bar{c}}^{*+}$ production for the $C = 0, S = 0$ resonances that we have

(I, S)	z_R (MeV)	g_a			
$(1/2, 0)$		$\bar{D}\Sigma_c$	$\bar{D}\Lambda_c^+$	$\eta_c N$	
	$4265 - 11.6i$	$2.96 - 0.21i$	$-0.08 + 0.06i$	$-0.94 + 0.03i$	
		2.97	0.10	0.94	
$(0, -1)$		$\bar{D}_s\Lambda_c^+$	$\bar{D}\Xi_c$	$\bar{D}\Xi'_c$	$\eta_c\Lambda$
	$4210 - 2.9i$	$1.42 - 0.03i$	$3.28 - 0.002i$	$-0.15 + 0.13i$	$0.57 + 0.04i$
		1.42	3.28	0.19	0.57
	$4398 - 8.0i$	$0.01 + 0.004i$	$0.06 - 0.02i$	$2.75 - 0.15i$	$-0.73 - 0.07i$
		0.01	0.06	2.75	0.74

TABLE VII: Pole position, z_R and coupling constants, g_a , to various channels for the states from $PB \rightarrow PB$ including the $\eta_c N$ and $\eta_c\Lambda$ channel.

(I, S)	z_R (MeV)	Real axis		Γ_i
		M	Γ	
$(1/2, 0)$				$\eta_c N$
	$4265 - 11.6i$	4261	56.9	23.4
$(0, -1)$				$\eta_c\Lambda$
	$4210 - 2.9i$	4209	32.4	5.8
	$4398 - 8.0i$	4394	43.3	16.3

TABLE VIII: Pole position (z_R), mass (M), total width (Γ , including the contribution from the light meson and baryon channel) and the decay widths for the $\eta_c N$ and $\eta_c\Lambda$ channels (Γ_i). The unit are in MeV

obtained from the pseudoscalar baryon interaction. Since one important decay channel of the $N_{c\bar{c}}^*$ is πN , we evaluate the cross section for the mechanism depicted in the Feynman diagram of Fig. 5.

The coupling of the $N_{c\bar{c}}^* \rightarrow \pi^0 p$ is obtained projecting over $\pi^0 p$ the isospin state $I = 1/2$, which provides the isospin coefficient $C_I = \sqrt{1/3}$. The coupling $N_{c\bar{c}}^* \rightarrow \pi N$ we get from the

(I, S)	z_R	g_a			
$(1/2, 0)$		$\bar{D}^*\Sigma_c$	$\bar{D}^*\Lambda_c^+$	$J/\psi N$	
	$4415 - 9.5i$	$2.83 - 0.19i$	$-0.07 + 0.05i$	$-0.85 + 0.02i$	
		2.83	0.08	0.85	
$(0, -1)$		$\bar{D}_s^*\Lambda_c^+$	$\bar{D}^*\Xi_c$	$\bar{D}^*\Xi'_c$	$J/\psi\Lambda$
	$4368 - 2.8i$	$1.27 - 0.04i$	$3.16 - 0.02i$	$-0.10 + 0.13i$	$0.47 + 0.04i$
		1.27	3.16	0.16	0.47
	$4547 - 6.4i$	$0.01 + 0.004i$	$0.05 - 0.02i$	$2.61 - 0.13i$	$-0.61 - 0.06i$
		0.01	0.05	2.61	0.61

TABLE IX: Pole position (z_R) and coupling constants (g_a) to various channels for the states from $PB \rightarrow PB$ including the $J/\psi N$ and $J/\psi\Lambda$ channels.

(I, S)	z_R	Real axis		Γ_i
		M	Γ	
$(1/2, 0)$				$J/\psi N$
	$4415 - 9.5i$	4412	47.3	19.2
$(0, -1)$				$J/\psi\Lambda$
	$4368 - 2.8i$	4368	28.0	5.4
	$4547 - 6.4i$	4544	36.6	13.8

TABLE X: Pole position (z_R), mass (M), total width (Γ , including the contribution from the light meson and baryon channel) and the decay widths for the $J/\psi N$ and $J/\psi\Lambda$ channels (Γ_i). The unit are in MeV

partial decay width of the $N_{c\bar{c}}^*$ into this channel, $\Gamma_{\pi N}$

$$g_{N_{c\bar{c}}^* \rightarrow \pi N}^2 = \frac{2\pi M_{N_{c\bar{c}}^*} \Gamma_{\pi N}}{M_N p_\pi^{\text{on}}} \quad (29)$$

with $p_\pi^{\text{on}} = \lambda^{1/2}(M_{N_{c\bar{c}}^*}^2, m_\pi^2, M_N^2)/2M_{N_{c\bar{c}}^*}$, the value of the on-shell pion momentum from the $N_{c\bar{c}}^* \rightarrow \pi N$ decay. By taking the standard πNN vertex, $V_{\pi NN} = ig_\pi \gamma_5 \tau^\lambda$ ($g_\pi \simeq 13$), we

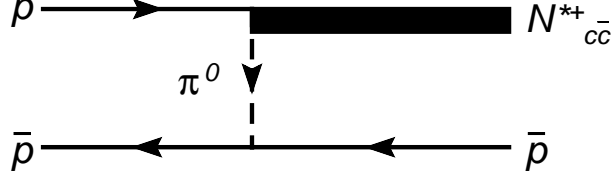


FIG. 5: The $p\bar{p} \rightarrow N_{c\bar{c}}^{*+} \bar{p}$ mechanism.

obtain

$$\frac{d\sigma_{p\bar{p} \rightarrow N_{c\bar{c}}^{*+} \bar{p}}}{d\cos\theta} = \frac{g_\pi^2}{4} \frac{M_X^2}{s} \frac{\Gamma_{\pi N} C_I^2}{p_\pi^{\text{on}}} \frac{2p \cdot p' - 2M^2}{(2M^2 - \sqrt{s}E(p') + 2\vec{p} \cdot \vec{p}')^2} \frac{p'}{p} \quad (30)$$

where p, p' are the initial, final momenta of the \bar{p} in the center of mass frame (of the order of 2570, 620 MeV/c for $M_X \simeq 4300$ MeV). The biggest cross section corresponds to the forward \bar{p} direction, which is the most indicated for the search. If we are interested in searching for these resonances, looking for \bar{p} forward is the most recommendable measurement and one should look for a bump into the $d\sigma/d\cos\theta dM_I^2$ magnitude, where M_I is the invariant mass of the πN coming from the decay of the produced $N_{c\bar{c}}^{*+}$ state. Assuming a Lorentzian shape for this resonance, with total width $\Gamma_{N_{c\bar{c}}^{*+}}$, we would obtain at the peak of the πN distribution

$$\frac{d\sigma_{p\bar{p} \rightarrow N_{c\bar{c}}^{*+} (4265) \bar{p} \rightarrow \pi N \bar{p}}}{d\cos\theta dM_I^2} = \frac{1}{\pi} \frac{1}{M_{N_{c\bar{c}}^{*+}} \Gamma_{\text{tot}}} \frac{d\sigma_{p\bar{p} \rightarrow N_{c\bar{c}}^{*+} \bar{p}}}{d\cos\theta} \frac{\Gamma_{\pi N}}{\Gamma_{\text{tot}}} \quad (31)$$

which leads to the following cross section: $0.13 \mu\text{b}/\text{GeV}^2$ for $N_{c\bar{c}}^{*+}(4265)$.

In the above calculation, we did not consider the form factor for the πNN vertex. The form factor is:

$$F_{pp\pi} = \frac{\Lambda_\pi^2 - m_\pi^2}{\Lambda_\pi^2 - p_\pi^2}. \quad (32)$$

with the $\Lambda_\pi = 1.3\text{GeV}$. We can multiply by $F_{pp\pi}^2$ the cross section in the Eq. (31) and we find about $0.05 \mu\text{b}/\text{GeV}^2$.

Because in such high energy transfer reaction the one-pion exchange with the monopole off-shell form factor of Eq.(32) may not be a good approximation, here we also make a calculation with the Reggeon exchange. Using a Reggeon propagator $R_\pi(s, t)$ [44] instead of the usual pion propagator. Then the Eq.(30) becomes

$$\frac{d\sigma_{p\bar{p} \rightarrow N_{c\bar{c}}^{*+} \bar{p}}}{d\cos\theta} = \frac{g_\pi^2}{4} \frac{M_X^2}{s} \frac{\Gamma_{\pi N} C_I^2}{p_\pi^{\text{on}}} (\sqrt{s}E(p') - 2pp'\cos\theta - 2M_N^2) |R_\pi(s, t)|^2 \frac{p'}{p}, \quad (33)$$

where

$$R_\pi(s, t) = -\frac{\pi}{2}\alpha'_{pi}(t)\exp(-i\frac{\pi}{2}\alpha_\pi(t))\frac{(s/s_0)^{\alpha_\pi(t)}}{\sin(\frac{\pi}{2}\alpha_\pi(t))\Gamma(\frac{\alpha_\pi(t)}{2} + 1)}, \quad (34)$$

$$\alpha_\pi(t) = -0.015 + 0.72t, \quad (35)$$

$$\alpha'_\pi(t) = 0.72, \quad (36)$$

$$t = 2M_N^2 - \sqrt{s}E(p') + 2pp'\cos\theta, \quad (37)$$

with the slope parameter in the units of (GeV^{-2}) . When $t \rightarrow m_\pi^2$, we can get $\alpha_\pi = 0$ and $R_\pi \sim \frac{1}{m_\pi^2 - t}$. From Ref.[44], the order of s_0 is about $2 - 20 GeV^{-2}$. To narrow down its range, we use the information of pp collision with $\sqrt{s} < 3 GeV$ where the one-pion exchange can reproduce experimental data reasonably well [45]. Demanding the Reggeon propagator to give similar results as the usual π propagator for $\sqrt{s} < 3 GeV$, we have $s_0 \simeq 5 - 10 GeV^{-2}$. Then by using Reggeon propagator for the maximum PANDA energy $\sqrt{s} < 5.47 GeV$, we get the cross section to be about $0.006 \sim 0.017 \mu b/GeV^2$ corresponding to $s_0 = 5 \sim 10 GeV^{-2}$. This is about a factor $3 \sim 9$ smaller than the result by one-pion exchange.

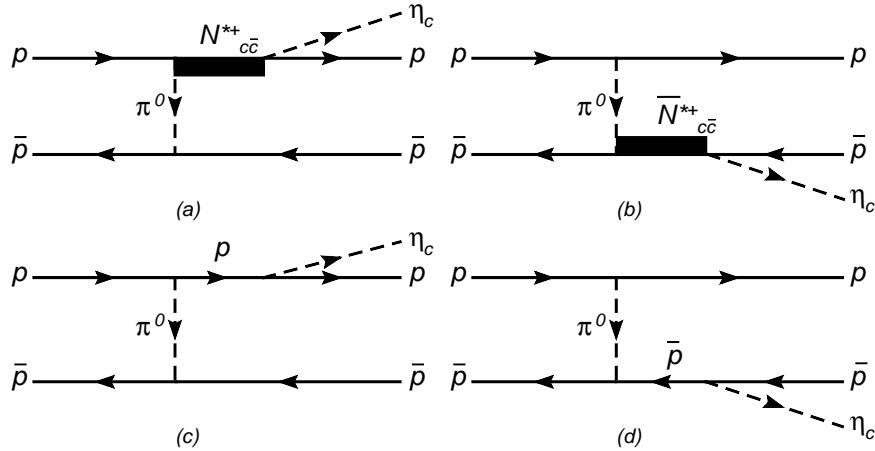


FIG. 6: The different Feynman diagrams of the reaction $p\bar{p} \rightarrow p\bar{p}\eta_c$

Then we can estimate the cross section of $p\bar{p} \rightarrow p\bar{p}\eta_c$. The different Feynman diagrams for this reaction are shown in the Fig. 6. Using Eq. (31) and $\Gamma_{\eta_c p}$ of the resonance instead of $\Gamma_{\pi N}$ we can obtain the differential cross section at the peak of the resonance, corresponding to the resonant mechanism of Fig. 6 a), and it is about $0.8 \mu b/GeV^2$ without form factor and $0.3 \mu b/GeV^2$ with the form factor, and $0.04 \sim 0.10 \mu b/GeV^2$ with the Reggeon propagator. This magnitude is of about the same order of magnitude as typical cross sections measured

for $d\sigma/d\cos\theta dM_I^2$ in the $pd \rightarrow pd\pi^0\pi^0$ or $pp \rightarrow d\pi^+\pi^0$ reaction [46, 47]. In order to see the role played by the hidden charm resonance in this process we can compare it with the cross section coming from a standard mechanism of Fig. 6(c,d). The vertex of $pp\eta_c$ is used by

$$\mathcal{L}_{\eta_c p\bar{p}} = g_{\eta_c p\bar{p}} \bar{u}_p \gamma^\mu \gamma^5 \partial_\mu \psi_{\eta_c} v_{\bar{p}}, \quad (38)$$

where $g_{\eta_c p\bar{p}}$ can be calculated from the reaction $\eta_c \rightarrow p\bar{p}$ by

$$g_{\eta_c p\bar{p}} = \sqrt{\frac{\pi \Gamma_{\eta_c} Br_{\eta_c p\bar{p}}}{|p_p^{on}| m_p^2}}. \quad (39)$$

where the $p_p^{on} = \lambda^{1/2}(m_{\eta_c}^2, M_p^2, M_{\bar{p}}^2)/2m_{\eta_c}$ the value of the on-shell p momentum from the $\eta_c \rightarrow p\bar{p}$ decay. And the width $\Gamma_{\eta_c} = 26.7 MeV$ and the branch ratio $Br_{\eta_c p\bar{p}} = 1.3 \times 10^{-3}$ are both from PDG. The form factor of the vertex $NN\pi$ is also used Eq.(32). We also add the form factors for $N_{c\bar{c}}^*$ and p exchange in the Fig.6:

$$F_p = \frac{\Lambda_p^4}{\Lambda_p^4 + (p_p^2 - m_p^2)^2}, \quad (40)$$

$$F_{N_{c\bar{c}}^*} = \frac{\Lambda_N^4}{\Lambda_N^4 + (p_{N_{c\bar{c}}^*}^2 - m_{N_{c\bar{c}}^*}^2)^2}. \quad (41)$$

Here $\Lambda_p = \Lambda_N = 0.8 GeV$.

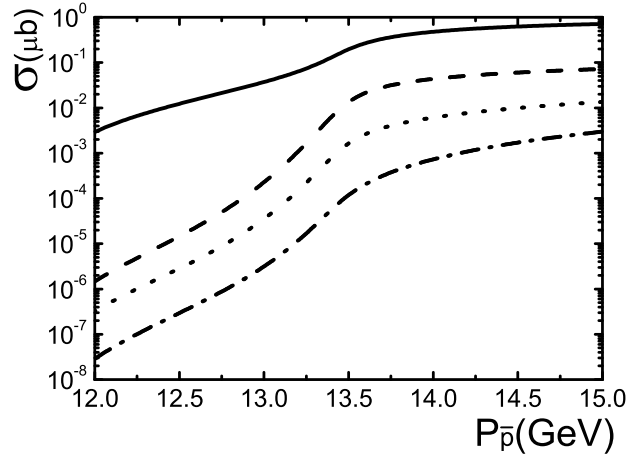


FIG. 7: The total cross section vs the beam momentum of \bar{p} for $p\bar{p} \rightarrow p\bar{p}\eta_c$. The solid and dashed lines are calculated by one-pion exchange without and with form factors, respectively. The dot-dashed and dotted lines are results by Reggeon propagator with $s_0 = 5$ and $10 GeV^{-2}$, respectively.

Through the calculation, the contributions from Fig. 6 (c), (d) are very small, almost $10^{-4}\mu b$, the main contribution comes from the $N_{c\bar{c}}^*$. The total cross section is about $0.0029\mu b$, $0.013\mu b$, $0.072\mu b$ and $0.71\mu b$ for a \bar{p} beam of 15 GeV/c as shown in Fig.7, corresponding to the Reggeon propagator with $s_0 = 5 \text{ GeV}^{-2}$ and $s_0 = 10 \text{ GeV}^{-2}$, the usual π propagator with and without form factors. Note that the integrated cross section involves finite angles, rather than zero in the forward direction considered before, where the effect of the form factor is more important. The Dalitz plot, the invariant mass spectrum of $p\eta_c$, $\bar{p}\eta_c$ and $p\bar{p}$ are all shown in Fig. 8 where the peaks of $N^*(4269)$ are very clear.

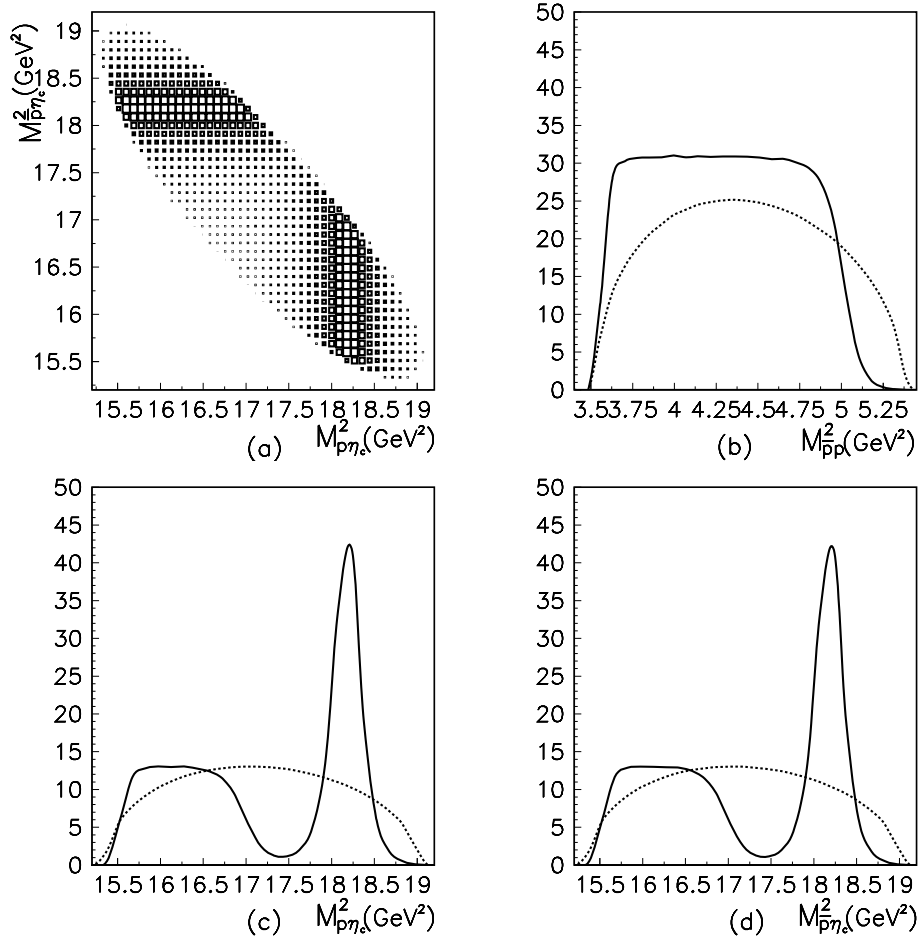


FIG. 8: The Dalitz plot(a), the invariant mass spectrum of $p\bar{p}$ (b), $p\eta_c$ (c) and $\bar{p}\eta_c$ (d) for the reaction $p\bar{p} \rightarrow p\bar{p}\eta_c$ at the beam momentum of \bar{p} being 14.00GeV at lab system.

B. J/ψ production in $\bar{p}p \rightarrow \bar{p}pJ/\psi$.

Another estimate that we want to do is the cross section for J/ψ production in the $\bar{p}p \rightarrow \bar{p}pJ/\psi$ reaction around the energy of the $N^*(4265)$ excitation. We use again Eq. (31) but we need to evaluate $\Gamma_{J/\psi p}$. This requires a different formalism to the one used so far. The mechanism for $R \rightarrow J/\psi p$ is obtained by analogy to the work done in [33, 34] where the transition from vector - vector to pseudoscalar - pseudoscalar states is done. Concretely, given the fact that the $N_{c\bar{c}}^{*+}(4265)$ is basically a $\bar{D}\Sigma_c$ molecule in our approach, we obtain the coupling of the resonance $N_{c\bar{c}}^{*+}(4265)$ to $J/\psi p$ through the diagram of Fig. 9.

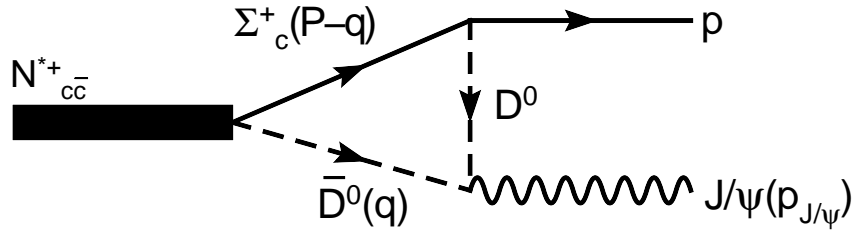


FIG. 9: pJ/ψ going to the resonance $N_{c\bar{c}}^{*+}(4265)$.

This diagram requires the coupling of $N_{c\bar{c}}^{*+}(2465)$ to the $\bar{D}\Sigma_c$ state in $I = 1/2$, and the transition $J/\psi p \rightarrow \bar{D}\Sigma_c$ which is mediated by the \bar{D} meson that comes from the coupling of J/ψ to $D\bar{D}$. The diagram also involves the $DN\Sigma_c$ coupling which has been studied in [48].

The $J/\psi \rightarrow D\bar{D}$ coupling can be obtained from the Lagrangian

$$\mathcal{L}_{PPV} = -ig\langle V^\mu [P, \partial_\mu P] \rangle, \quad (42)$$

used in Section II, with $g = M_V/2f$ and $f = 93$ MeV, which leads to

$$-it_{J/\psi D\bar{D}} = i2g q_\mu \epsilon^\mu. \quad (43)$$

The vertex $DN\Sigma_c$ is obtained from [48] and has the form

$$-iV_{D^0 p \Sigma_c^+} = \vec{\sigma} \cdot \vec{q}' \left(1 - \frac{q'^0}{2M'}\right) \beta \frac{D-F}{2f} \quad (44)$$

with $\beta = 1$ and q'^0 , \vec{q}' , the incoming energy, momentum of the D meson and M' the mass of the Σ_c . For D and F we take the standard values $D = 0.8$ and $F = 0.46$ [49–51]. Thus,

$$-it_{D^0 p \Sigma_c^+} = \frac{0.26}{2f} \vec{\sigma} \cdot \vec{q}' \quad (45)$$

We need the $I = 1/2$ state of $\bar{D}\Sigma_c$ given with our phase convention by

$$|\bar{D}\Sigma_c; 1/2, 1/2\rangle = \sqrt{\frac{2}{3}}D^{-\Sigma_c^{++}} + \frac{1}{\sqrt{3}}\bar{D}^0\Sigma_c^+ . \quad (46)$$

The other possible vertex, the $D^+p\Sigma_c^{++}$ vertex, is $\sqrt{2}$ times the $D^0p\Sigma_c^+$ one. With all these ingredients one obtains

$$t_{J/\psi p \rightarrow R} = 2\sqrt{3}g \int \frac{d^4q}{(2\pi)^4} \frac{0.26}{2f} \vec{\epsilon} \cdot \vec{q} \vec{\sigma} \cdot \vec{q} \frac{M_{\Sigma_c}}{E_{\Sigma_c}(q)} \frac{1}{q^2 - m_D^2 + i\epsilon} \\ \times \frac{1}{(p_J - q)^2 - m_D^2 + i\epsilon} \frac{1}{P^0 - q^0 - E_{\Sigma_c}(q) + i\epsilon} F(q) , \quad (47)$$

where we use a form factor $F(q) = \frac{\Lambda^2}{\Lambda^2 + q^2}$ with $\Lambda = 1.05$ GeV [48] in the integral of Eq. (47). Upon neglecting the small three momenta $\vec{p}_{J/\psi}$ compared to the J/ψ mass and performing the q^0 integral, Eq. (47) can be written as

$$-it_{J/\psi p \rightarrow R} = -\frac{1}{\sqrt{3}} \frac{0.26}{f} g \vec{\sigma} \cdot \vec{\epsilon} \int \frac{d^3q}{(2\pi)^3} \vec{q}^2 \frac{M_{\Sigma_c}}{E_{\Sigma_c}(q)} \frac{1}{2\omega_D(q)} \frac{1}{p_J^0 + 2\omega_D(q)} \frac{1}{p_J^0 - 2\omega_D(q)} \\ \times \frac{1}{P^0 - p_J^0 - \omega_D(q) - E_{\Sigma_c}(q)} \frac{1}{P^0 - \omega_D(q) - E_{\Sigma_c}(q) + i\epsilon} \\ \times \{2(P^0 - \omega_D(q) - E_{\Sigma_c}(q) - p_J^0 - 2\omega_D(q))\} , \quad (48)$$

where $\omega_D(q) = \sqrt{q^2 + m_D^2}$ and $E_{\Sigma_c}(q) = \sqrt{q^2 + m_{\Sigma_c}^2}$. The width of $N_{c\bar{c}}^{*+} \rightarrow J/\psi p$ is now given by

$$\Gamma = \frac{1}{2\pi} \frac{M_p}{M_R} p |\tilde{t}_{J/\psi p \rightarrow R}|^2 \quad (49)$$

where $\tilde{t}_{J/\psi p \rightarrow R}$ means $t_{J/\psi p \rightarrow R}$ omitting the $\vec{\sigma} \cdot \vec{\epsilon}$ operator. We take $P^0 = M_R = 4265$ MeV and $p = \lambda^{1/2}(M_R^2, M_{J/\psi}^2, M_p^2)/2M_R$, while M_p stands for the mass of the proton. By using the form factor of [48], we get

$$\Gamma_{R \rightarrow J/\psi p} = 0.01 \text{ MeV} , \quad (50)$$

with admitted uncertainties of the order of a factor two. Since $\Gamma_{\pi N}$ of the $N_{c\bar{c}}^{*+}(4265)$ was of the order of 3.8 MeV, now the cross section is about a factor 400 smaller than before. Yet, the fact that the background for $J/\psi p$ production is also smaller might compensate for it. But, from what we have said before, the cross section for $\eta_c p$ production is much bigger.

On the other hand, for the resonances made out by VB , the $J/\psi p$ production cross sections are larger. One can repeat the calculations in this case. We sketch the derivation below.

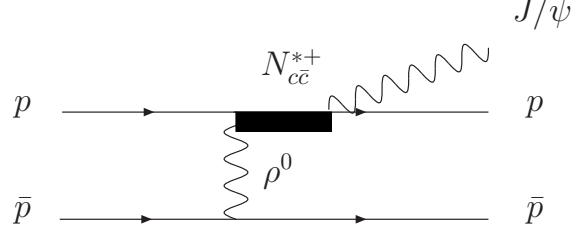


FIG. 10: The $p\bar{p} \rightarrow J/\psi p\bar{p}$ mechanism throughout the resonance $N_{c\bar{c}}^{*+}$

We shall make the estimate based upon the mechanism of the Feynman diagram of Fig. 10, and we will consider the resonance $N_{c\bar{c}}^*(4418)$ coming from the interaction of vector mesons with baryons, one of which channels is $J/\psi p$, which was considered in the Subsection III. C as seen in Table IX. By adding this new channel we found $g_{XJ/\psi N} = 0.85$. Assuming the dominant decay channels of N^* as ρN (For $\rho^0 N$, it should be added $C_I = 1/\sqrt{3}$) and dominance of the γ^0 term in the $\rho^0 p\bar{p}$ vertex, which goes then as $g\gamma^0/\sqrt{2}$, and $g = M_v/2f$, we obtain now

$$\frac{d\sigma_{p\bar{p} \rightarrow N_{c\bar{c}}^*(4418)\bar{p}}}{d\cos\theta} = \frac{g^2 M_X^2 \Gamma_{\rho N} C_I^2}{4 s p_\rho^{\text{on}}} \frac{E(p')E(p) + \vec{p} \cdot \vec{p}' + M^2}{(2M^2 - \sqrt{s}E(p') + 2\vec{p} \cdot \vec{p}' - M_\rho^2)^2} \frac{p'}{p} \quad (51)$$

with p', p the \bar{p} outgoing, incoming momenta in the center of mass frame, and p_ρ^{on} the ρ momentum in the $N_{c\bar{c}}^*(4418)$ decay into ρN . By means of Eq. (51) and the width of $N_{c\bar{c}}^*(4418) \rightarrow J/\psi p$, we can calculate the cross section of the reaction $p\bar{p} \rightarrow J/\psi p\bar{p}$ multiplying the cross section of Eq. (51) by the branching ratio of the resonance for the decay into $J/\psi p$. As one can see in Fig. 11, this cross section is of the order of $2 \sim 37 \text{ nb}$ for a \bar{p} beam of $15 \text{ GeV}/c$, depending on whether one includes or not the form factors. And for the dashed line, we also give the form factor for the $NN\rho$ vertex and $N_{c\bar{c}}^*(4418)$ as follows:

$$F_{pp\pi} = \frac{\Lambda_\rho^2 - m_\rho^2}{\Lambda_\rho^2 - p_\rho^2}. \quad (52)$$

$$F_{N_{c\bar{c}}^*} = \frac{\Lambda_N^4}{\Lambda_N^4 + (p_{N^*(4418)}^2 - m_{N^*(4418)}^2)^2}. \quad (53)$$

with $\Lambda_\rho = 1.3 \text{ GeV}$ and $\Lambda_N = 0.8 \text{ GeV}$.

This cross section is larger than the one we would obtain from the standard mechanism of Fig. 12, which can be evaluated in analogy to the case of Fig. 6. Once again, using Eq. (31) and $\Gamma_{J/\psi p}$ of the resonance instead of $\Gamma_{\pi N}$ we can obtain the differential cross section of the peak of the resonance: $6 \sim 50 \text{ nb}/\text{GeV}^2$.

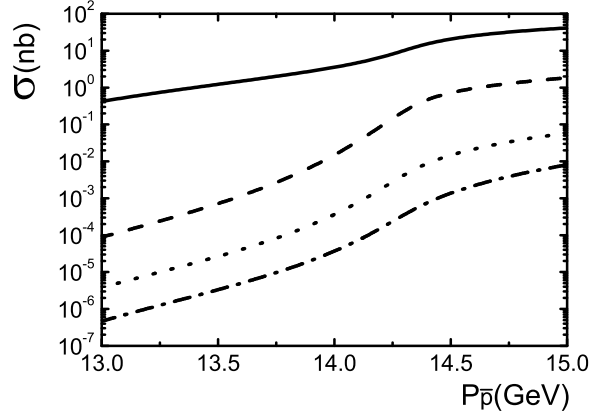


FIG. 11: The total cross section vs the \bar{p} beam momentum for $p\bar{p} \rightarrow p\bar{p}J/\psi$. The solid and dashed lines are calculated by ρ -meson exchange without and with form factors, respectively. The dot-dashed and dotted lines are calculated by Reggeon propagator with $s_0 = 5$ and 8 GeV^{-2} , respectively.

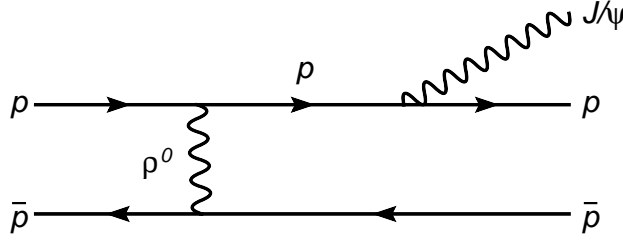


FIG. 12: The standard $p\bar{p} \rightarrow J/\psi p\bar{p}$ mechanism.

For the same reasons as for the $N_{cc}^*(4265)$ production, we also consider the Reggeon exchange here. The Eq.(51) becomes as follows:

$$\frac{d\sigma_{p\bar{p} \rightarrow N_{cc}^*(4418)\bar{p}}}{d\cos\theta} = \frac{g^2 M_X^2 \Gamma_{\rho N} C_I^2}{4 s p_\rho^{\text{on}}} (E(p')E(p) + pp' \cos\theta + M_N^2) |R_\rho(s, t)|^2 \frac{p'}{p} \quad (54)$$

where

$$R_\rho(s, t) = -\frac{\pi}{2} \alpha'_\rho(t) \exp(-i\frac{\pi}{2} \alpha_\rho(t)) \frac{(s/s_0)^{\alpha_\rho(t)-1}}{\cos(\frac{\pi}{2} \alpha_\rho(t)) \Gamma(\frac{\alpha_\rho(t)}{2} + \frac{1}{2})} \quad (55)$$

$$\alpha_\rho(t) = 0.5 + 0.83t \quad (56)$$

$$\alpha'_\rho(t) = 0.83 \quad (57)$$

$$t = 2M_N^2 - \sqrt{s}E(p') + 2pp' \cos\theta \quad (58)$$

When $t \rightarrow m_\rho^2$, $\alpha_\rho = 1$ and $R_\rho \sim \frac{1}{m_\rho^2 - t}$. For the estimation the value of s_0 is taken to be from 5 GeV^{-2} to 8 GeV^{-2} , such that $|R_\rho(s, t)|^2$ gives almost the same results as $\frac{1}{(m_\rho^2 - t)^2}$ when $\sqrt{s} < 3 \text{ GeV}$. By using Reggeon propagator, the total cross section is about $0.008 \sim 0.06 \text{ nb}$ for a \bar{p} beam of $15 \text{ GeV}/c$. This is about two orders of magnitude smaller than the result by ρ -meson exchange.

From the calculation above, we find that the cross section of this reaction is about two orders of magnitude smaller than that of the reaction $p\bar{p} \rightarrow p\bar{p}\eta_c$, but it could be also appropriate to find $N^*(4418)$ because the J/ψ has a large branching ratio to decay into lepton channels which are much easier to detect than hadron channels.

Finally let us discuss the possibility of measurement of this reaction in the experiments. The PANDA(anti-Proton Annihilation at Darmstadt) Collaboration will study the $p\bar{p}$ reaction at FAIR, with the \bar{p} beam energy in the range of 1.5 to $15 \text{ GeV}/c$ and luminosity of about $10^{31} \text{ cm}^{-2} \text{ s}^{-1}$ [52]. The range of the beam energy is very suitable to find the $N^*(4265)$ and the $N^*(4418)$, with cross sections estimated to be about 70 nb and 2 nb by the one-meson exchange propagators with off-shell form factors, which corresponds to an event production rate of 60000 and 1700 per day at PANDA/FAIR, or about 10 nb and 0.02 nb by the Reggeon propagators, which corresponds to an event production rate of 9000 and 20 per day at PANDA/FAIR. There is a 4π solid angle detector with good particle identification for charged particles and photons at PANDA/FAIR. For the $p\bar{p} \rightarrow p\bar{p}\eta_c$ reaction, if p and \bar{p} are identified, then the η_c can be easily reconstructed from the missing mass spectrum against p and \bar{p} . It is the same as the reaction $p\bar{p} \rightarrow p\bar{p}J/\psi$. So this reaction should be accessible at PANDA/FAIR.

V. SUMMARY

In summary, we find six states from PB and VB channels by using the local hidden gauge Lagrangian in combination with unitary techniques in coupled channels. All of these states have large $c\bar{c}$ components, so their masses are all larger than 4200 MeV . The width of these states decaying to light meson and baryon channels without $c\bar{c}$ components are all very small. On the other hand, the $c\bar{c}$ meson - light baryon channels are also considered to contribute to the decay width to these states. Then $\eta_c N$ and $\eta_c \Lambda$ are added to the PB channels, while $J/\psi N$ and $J/\psi \Lambda$ are added in the VB channels. The decay widths to these

channels are not negligible, in spite of the small phase space for the decay, because the exchange D^* (or D_s^*) mesons were less off-shell than the corresponding one in the decay to light meson - light baryon channels. The total width of these states are still very small. We made some estimates of cross sections for production of these resonances at the upcoming FAIR facility. The cross section of the reaction $p\bar{p} \rightarrow p\bar{p}\eta_c$ and $p\bar{p} \rightarrow p\bar{p}J/\psi$ are about $10 \sim 70nb$ and $0.02 \sim 2nb$, in which the main contribution comes from the predicted $N_{c\bar{c}}^*(4265)$ and $N_{c\bar{c}}^*(4418)$ states, respectively. With this theoretical results, one can estimate about $9000 \sim 60000$ and $20 \sim 1700$ events per day at the PANDA/FAIR facility, respectively.

The predicted $N_{c\bar{c}}^*$ and $\Lambda_{c\bar{c}}^*$ can be also looked for by many other processes, such as $ep \rightarrow eN_{c\bar{c}}^*$ at JLab's 12 GeV upgrade, $Kp \rightarrow \Lambda_{c\bar{c}}^*$ at JPARC, pp collisions, etc.

Acknowledgments

We thank Li-sheng Geng and Feng-kun Guo for useful discussions. This work is partly supported by DGICYT Contract No. FIS2006-03438, the Generalitat Valenciana in the project PROMETEO, the EU Integrated Infrastructure Initiative Hadron Physics Project under contract RII3-CT-2004-506078, the National Natural Science Foundation of China (NSFC) under grants Nos. 10875133, 10821063, 11035006, the Chinese Academy of Sciences under project No. KJCX2-EW-N01, and the Ministry of Science and Technology of China (2009CB825200).

Appendix A: The C_{ab} coefficients

In this Appendix we give the coefficients C_{ab} in Eqs. (13, 14, 25,27) for the several (I, S) sectors studied in this work.

TABLE XI: Coefficients C_{ab} in the Eq. (13, 25) for the PB system in the sector $I = 3/2, S = 0$.

	$\bar{D}\Sigma_c$	πN	$K\Sigma$
$\bar{D}\Sigma_c$	2	-1	1

TABLE XII: Coefficients C_{ab} in the Eq. (13, 25, 27) for the PB system in the sector $I = 1/2$, $S = 0$.

	$\bar{D}\Sigma_c$	$\bar{D}\Lambda_c^+$	$\eta_c N$	πN	ηN	$\eta' N$	$K\Sigma$	$K\Lambda$
$\bar{D}\Sigma_c$	-1	0	$-\sqrt{3/2}$	-1/2	$-1/\sqrt{2}$	1/2	1	0
$\bar{D}\Lambda_c^+$		1	$\sqrt{3/2}$	-3/2	$1/\sqrt{2}$	-1/2	0	1

TABLE XIII: Coefficients C_{ab} in the Eq. (13, 25) for the PB system in the sector $I = 1/2$, $S = -2$.

	$\bar{D}_s \Xi'_c$	$\bar{D}_s \Xi_c$	$\bar{D}\Omega_c$	$\pi \Xi$	$\bar{K}\Sigma$	$\eta \Xi$	$\eta' \Xi$	$\bar{K}\Lambda$
$\bar{D}_s \Xi'_c$	1	0	$\sqrt{2}$	0	$\sqrt{3}/2$	$1/\sqrt{6}$	$1/\sqrt{3}$	$-\sqrt{3}/2$
$\bar{D}_s \Xi_c$		1	0	0	-3/2	$1/\sqrt{2}$	1	1/2
$\bar{D}\Omega_c$			0	$\sqrt{3/2}$	0	$-1/\sqrt{3}$	$1/\sqrt{6}$	0

TABLE XIV: Coefficients C_{ab} in the Eq. (13, 25) for the PB system in the sector $I = 1$, $S = -1$.

	$\bar{D}_s \Sigma_c$	$\bar{D}\Xi'_c$	$\bar{D}\Xi_c$	$\pi \Sigma$	$\pi \Lambda$	$\eta \Sigma$	$\eta' \Sigma$	$\bar{K}N$	$K \Xi$
$\bar{D}_s \Sigma_c$	0	$\sqrt{2}$	0	0	0	$-1/\sqrt{3}$	$\sqrt{2/3}$	-1	0
$\bar{D}\Xi'_c$		1	0	$1/\sqrt{2}$	$-\sqrt{3}/2$	$1/\sqrt{6}$	$1/2\sqrt{3}$	0	$1/\sqrt{2}$
$\bar{D}\Xi_c$			1	$-\sqrt{3/2}$	1/2	$-1/\sqrt{2}$	-1/2	0	$\sqrt{3/2}$

TABLE XV: Coefficients C_{ab} in the Eq. (13, 25, 27) for the PB system in the sector $I = 0$, $S = -1$.

	$\bar{D}_s \Lambda_c^+$	$\bar{D} \Xi_c$	$\bar{D} \Xi'_c$	$\eta_c \Lambda$	$\pi \Sigma$	$\eta \Lambda$	$\eta' \Lambda$	$\bar{K} N$	$K \Xi$
$\bar{D}_s \Lambda_c^+$	0	$-\sqrt{2}$	0	1	0	$1/\sqrt{3}$	$\sqrt{2/3}$	$-\sqrt{3}$	0
$\bar{D} \Xi_c$		-1	0	$1/\sqrt{2}$	$-3/2$	$1/\sqrt{6}$	$-1/2\sqrt{3}$	0	$\sqrt{3/2}$
$\bar{D} \Xi'_c$			-1	$-\sqrt{3/2}$	$\sqrt{3/2}$	$-1/\sqrt{2}$	$1/2$	0	$1/\sqrt{2}$
$\eta_c \Lambda$				0	0	0	0	0	0

TABLE XVI: Coefficients C_{ab} in the Eq. (13, 25) for the PB system in the sector $I = 0$, $S = -3$.

	$\bar{D}_s \Sigma_c$	$\bar{K} \Xi$
$\bar{D}_s \Sigma_c$	2	$\sqrt{2}$

TABLE XVII: Coefficients C_{ab} in the Eq. (14, 25) for the VB system in the sector $I = 3/2$, $S = 0$.

	$\bar{D}^* \Sigma_c$	ρN	$K^* \Sigma$
$\bar{D}^* \Sigma_c$	2	-1	1

TABLE XVIII: Coefficients C_{ab} in the Eq. (14, 25) for the VB system in the sector $I = 1/2$, $S = 0$.

	$\bar{D}^* \Sigma_c$	$\bar{D}^* \Lambda_c^+$	ρN	ωN	ϕN	$K^* \Sigma$	$K^* \Lambda$
$\bar{D}^* \Sigma_c$	-1	0	$-1/2$	$\sqrt{3}/2$	0	1	0
$\bar{D}^* \Lambda_c^+$		1	$-3/2$	$-\sqrt{3}/2$	0	0	1

TABLE XIX: Coefficients C_{ab} in the Eq. (14, 25) for the VB system in the sector $I = 1/2, S = -2$.

	$\bar{D}_s^* \Xi'_c$	$\bar{D}_s^* \Xi_c$	$\bar{D}^* \Omega_c$	$\rho \Xi$	$\bar{K}^* \Sigma$	$\omega \Xi$	$\phi \Xi$	$\bar{K}^* \Lambda$
$\bar{D}_s^* \Xi'_c$	1	0	$\sqrt{2}$	0	$\sqrt{3}/2$	0	$-1/\sqrt{2}$	$-\sqrt{3}/2$
$\bar{D}_s^* \Xi_c$		1	0	0	$-3/2$	0	$-\sqrt{3}/2$	$1/2$
$\bar{D}^* \Omega_c$			0	$\sqrt{3}/2$	0	$\sqrt{3}/2$	0	0

TABLE XX: Coefficients C_{ab} in the Eq. (14, 25) for the VB system in the sector $I = 1, S = -1$.

	$\bar{D}_s^* \Sigma_c$	$\bar{D}^* \Xi'_c$	$\bar{D}^* \Xi_c$	$\rho \Sigma$	$\rho \Lambda$	$\omega \Sigma$	$\phi \Sigma$	$\bar{K}^* N$	$K^* \Xi$
$\bar{D}_s^* \Sigma_c$	0	$\sqrt{2}$	0	0	0	0	-1	-1	0
$\bar{D}^* \Xi'_c$		1	0	$1/\sqrt{2}$	$-\sqrt{3}/2$	$-1/2$	0	0	$1/\sqrt{2}$
$\bar{D}^* \Xi_c$			1	$-\sqrt{3}/2$	$1/2$	$\sqrt{3}/2$	0	0	$\sqrt{3}/2$

TABLE XXI: Coefficients C_{ab} in the Eq. (14, 25) for the VB system in the sector $I = 0, S = -1$.

	$\bar{D}_s^* \Lambda_c^+$	$\bar{D}^* \Xi_c$	$\bar{D}^* \Xi'_c$	$\rho \Sigma$	$\omega \Lambda$	$\phi \Lambda$	$\bar{K}^* N$	$K^* \Xi$
$\bar{D}_s^* \Lambda_c^+$	0	$-\sqrt{2}$	0	0	0	-1	$-\sqrt{3}$	0
$\bar{D}^* \Xi_c$		-1	0	$-3/2$	$-1/2$	0	0	$\sqrt{3}/2$
$\bar{D}^* \Xi'_c$			-1	$\sqrt{3}/2$	$\sqrt{3}/2$	0	0	$1/\sqrt{2}$

TABLE XXII: Coefficients C_{ab} in the Eq. (14, 25) for the VB system in the sector $I = 0, S = -3$.

	$\bar{D}_s^* \Sigma_c$	$\bar{K}^* \Xi$
$\bar{D}_s^* \Sigma_c$	2	$\sqrt{2}$

[1] N. Kaiser, P. B. Siegel and W. Weise, Nucl. Phys. A **594**, 325 (1995) [arXiv:nucl-th/9505043].

- [2] E. Oset and A. Ramos, Nucl. Phys. A **635** (1998) 99
- [3] J. A. Oller and U. G. Meissner, Phys. Lett. B **500**, 263 (2001) .
- [4] C. Garcia-Recio, J. Nieves, E. Ruiz Arriola and M. J. Vicente Vacas, Phys. Rev. D **67**, 076009 (2003)
- [5] T. Hyodo, S. I. Nam, D. Jido and A. Hosaka, Phys. Rev. C **68**, 018201 (2003).
- [6] E. E. Kolomeitsev and M. F. M. Lutz, Phys. Lett. B **585** (2004) 243 .
- [7] S. Sarkar, E. Oset and M. J. Vicente Vacas, Nucl. Phys. A **750**, 294 (2005) [Erratum-ibid. A **780**, 78 (2006)] .
- [8] S. Sarkar, B. X. Sun, E. Oset and M. J. V. Vacas, Eur. Phys. J. A **44** 431(2010)
- [9] E. Oset and A. Ramos, Eur. Phys. J. A **44** 445(2010)
- [10] Riazuddin and Fayyazuddin, Phys. Rev. **147**, 1071 (1966).
- [11] J.J. Sakurai, Currents and mesons (University of Chicago Press, Chicago Il 1969)
- [12] N. Kaiser, P. B. Siegel and W. Weise, Phys. Lett. B **362**, 23 (1995) [arXiv:nucl-th/9507036].
- [13] T. Inoue, E. Oset and M. J. Vicente Vacas, Phys. Rev. C **65**, 035204 (2002) [arXiv:hep-ph/0110333].
- [14] J. Nieves and E. Ruiz Arriola, Phys. Rev. D **64**, 116008 (2001)
- [15] B. C. Liu and B. S. Zou, Phys. Rev. Lett. **96**, 042002 (2006) [arXiv:nucl-th/0503069]; ibid, **98**, 039102 (2007).
- [16] L. S. Geng, E. Oset, B. S. Zou and M. Doring, Phys. Rev. C **79**, 025203 (2009) [arXiv:0807.2913 [hep-ph]].
- [17] M. F. M. Lutz and C. L. Korpa, Phys. Lett. B **633**, 43 (2006) [arXiv:nucl-th/0510006].
- [18] J. Hofmann and M. F. M. Lutz, Nucl. Phys. A **763**, 90 (2005) [arXiv:hep-ph/0507071].
- [19] T. Mizutani and A. Ramos, Phys. Rev. C **74**, 065201 (2006)
- [20] L. Tolos, A. Ramos and T. Mizutani, Phys. Rev. C **77**, 015207 (2008) [arXiv:0710.2684 [nucl-th]].
- [21] C. Garcia-Recio, V. K. Magas, T. Mizutani, J. Nieves, A. Ramos, L. L. Salcedo and L. Tolos, Phys. Rev. D **79**, 054004 (2009) [arXiv:0807.2969 [hep-ph]].
- [22] M. Bando, T. Kugo, S. Uehara, K. Yamawaki and T. Yanagida, Phys. Rev. Lett. **54**, 1215 (1985).
- [23] M. Bando, T. Kugo and K. Yamawaki, Phys. Rept. **164**, 217 (1988).
- [24] M. Harada and K. Yamawaki, Phys. Rept. **381**, 1 (2003) [arXiv:hep-ph/0302103].

- [25] U. G. Meissner, Phys. Rept. **161**, 213 (1988).
- [26] J. J. Wu, R. Molina, E. Oset and B. S. Zou, arXiv:1007.0573 [nucl-th], Phys. Rev. Lett. (in press).
- [27] E. Oset *et al.*, arXiv:0911.2580
- [28] E. M. Haacke, J. W. Moffat and P. Savaria, J. Math. Phys. **17**, 2041 (1976).
- [29] P. S. J. McNamee and F. Chilton, Rev. Mod. Phys. **36**, 1005 (1964).
- [30] L. Roca, E. Oset and J. Singh, Phys. Rev. D **72**, 014002 (2005)
- [31] J. A. Oller and E. Oset, Phys. Rev. D **60**, 074023 (1999)
- [32] J. Nieves and E. Ruiz Arriola, Nucl. Phys. A **679**, 57 (2000)
- [33] R. Molina, D. Nicmorus and E. Oset, Phys. Rev. D **78**, 114018 (2008)
- [34] L. S. Geng and E. Oset, Phys. Rev. D **79**, 074009 (2009)
- [35] D. Gamermann, PhD Thesis, chapter 6, [http : //ific.uv.es/nucth/tesis_DanGam.pdf](http://ific.uv.es/nucth/tesis_DanGam.pdf)
- [36] E. E. Kolomeitsev, M. F. M. Lutz, Phys. Lett. **B582**, 39-48 (2004).
- [37] J. Hofmann, M. F. M. Lutz, Nucl. Phys. **A733**, 142-152 (2004).
- [38] F. -K. Guo, P. -N. Shen, H. -C. Chiang *et al.*, Phys. Lett. **B641**, 278-285 (2006).
- [39] D. Gamermann, E. Oset, D. Strottman *et al.*, Phys. Rev. **D76**, 074016 (2007).
- [40] D. Gamermann, E. Oset, Eur. Phys. J. **A33**, 119-131 (2007).
- [41] R. Molina, H. Nagahiro, A. Hosaka *et al.*, Phys. Rev. **D80**, 014025 (2009).
- [42] R. Molina, E. Oset, Phys. Rev. **D80**, 114013 (2009).
- [43] R. Molina and E. Oset, Phys. Rev. D **80**, 114013 (2009) [arXiv:0907.3043 [hep-ph]].
- [44] V. V. Anisovich and A. V. Sarantsev, Int. J. Mod. Phys. A **24**, 2481 (2009).
- [45] Z. Ouyang, J. J. Xie, B. S. Zou and H. S. Xu, Nucl. Phys. A **821**, 220 (2009)
- [46] M. Bashkanov *et al.*, Phys. Rev. Lett. **102**, 052301 (2009)
- [47] F. Kren *et al.* [CELSIUS/WASA Collaboration], Phys. Lett. B **684**, 110 (2010)
- [48] R. Molina, D. Gamermann, E. Oset and L. Tolos, Eur. Phys. J. A **42**, 31 (2009)
- [49] B. Borasoy, P. C. Bruns, U. G. Meissner and R. Nissler, Eur. Phys. J. A **34**, 161 (2007)
- [50] F. E. Close and R. G. Roberts, Phys. Lett. B **316**, 165 (1993)
- [51] B. Borasoy, Phys. Rev. D **59**, 054021 (1999)
- [52] J. G. Messchendorp [PANDA Collaboration], *In the Proceedings of 11th International Conference on Meson-Nucleon Physics and the Structure of the Nucleon (MENU 2007), Julich, Germany, 10-14 Sep 2007, pp 123*